



Research Paper

Experimental evaluation of a 3D printed air dehumidification system developed with green desiccant materials

Francisco Comino ^{a,*}, Pablo E. Romero ^a, Esther Molero ^a, Manuel Ruiz de Adana ^b^a Departamento de Mecánica, Escuela Politécnica Superior, Universidad de Córdoba, Campus de Rabanales, Antigua Carretera Nacional IV, km 396, 14071 Córdoba, Spain^b Departamento de Química-Física y Termodinámica Aplicada, Escuela Politécnica Superior, Universidad de Córdoba, Campus de Rabanales, Antigua Carretera Nacional IV, km 396, 14071 Córdoba, Spain

ARTICLE INFO

ABSTRACT

Keywords:

Green desiccant
Fixed-bed system
Adsorption
Fused filament fabrication
Organic materials

Energy-efficient dehumidification systems are necessary to reduce energy consumption and CO₂ emissions into the atmosphere. Desiccant systems could be an alternative to conventional air dehumidification systems based on direct-expansion units. In the present work, the main objective was to develop and experimentally evaluate a 3D printed desiccant system manufactured using green desiccant materials. Hence, the adsorbent capacity of three 3D printed desiccant materials were studied: polylactic acid (PLA), pine wood with PLA (PW-PLA) and olive pit with PLA (OP-PLA). The results showed that PW-PLA was the material with the highest adsorption capacity of those analysed, up to 12.7 % higher than OP-PLA. A fixed bed desiccant system was fabricated using PW-PLA filament and its latent energy performance was investigated under different inlet air conditions and low regeneration temperature, 50 °C. The evaluation of the energy performance of the 3D printed desiccant system revealed adequate moisture removal capacity values, up to 30 g/sm³, with low pressure drop, less than 552 Pa. These results show the promising potential of 3D printing and green desiccant materials for manufacturing ecological air dehumidification systems.

1. Introduction

A large percentage of world's energy consumption in buildings is due to indoor air handling, that is, to heating, ventilation and air conditioning (HVAC) systems [1]. In recent years, the efficiency of HVAC systems has improved significantly. However, these solutions have focused on the treatment of sensible heat, often overlooking the treatment of latent heat and how it affects people's comfort [2]. Recent studies have shown that the energy consumption associated with reducing air humidity could be greater than that of reducing air temperature [2]. Therefore, energy-efficient dehumidification systems are necessary to reduce energy consumption and consequently, reduce CO₂ emissions into the atmosphere.

Air dehumidification equipment based on direct expansion units are widely used for moisture treatment. Nevertheless, these units are highly dependent on electrical energy. Desiccant dehumidification systems could be an alternative to conventional dehumidification systems [3,4]. These elements adsorb moisture from an air stream achieving an area of low vapour pressure at the surface of the desiccant material [5]. There

are different types of desiccant systems, such as liquid spray-tower, fixed-bed, desiccant wheel or multiple vertical bed [5]. However, desiccant wheels and fixed beds have been the most used desiccant systems, mainly due to their high dehumidification capacity and simple design. Moreover, previous studies of desiccant systems have shown acceptable dehumidification values using low regeneration air temperatures [6–8]. This fact allows the use of low-temperature renewable energies as a heat source to thermally activate the desiccant material [9,10], such as solar thermal energy or biomass.

The most widely used desiccant material in these dehumidification systems was silica gel, due to its high moisture adsorption capacity [11]. Nevertheless, there are other desiccant materials with good capacity to remove moisture, such as zeolites [12], calcium chloride [13], polyvinyl alcohol [13], lithium chloride [14] or metal-organic frameworks [15]. Green desiccants, i.e., desiccants obtained from agricultural waste materials, have also been studied previously [16]. Some green desiccants studied with good adsorption capacity values were pine sawdust [17,18], olive pit [19] or rice husk [20]. These desiccant materials could be an environmentally friendly alternative to commercial desiccants. However, the moisture adsorption capacity was not studied in most of

* Corresponding author.

E-mail address: francisco.comino@uco.es (F. Comino).

| Nomenclature | | \hat{Y} | estimated output value |
|------------------|--|----------------------|--|
| a | estimated parameter | <i>Greek letters</i> | |
| b | thickness of the composite [m] | Δ | differential |
| D | diffusion coefficient [m^2/s] | η | efficiency [-] |
| h | enthalpy [kJ/kg] | ω | humidity ratio [kg/kg] |
| MRC | moisture removal capacity [mg/s] | θ | initial slope of a plot of $M(t)$ versus $t^{1/2}$ |
| MRC _a | accumulated moisture removal capacity [mg/s] | <i>Subscripts</i> | |
| \dot{m} | mass air flow rate [kg/s] | f | fan |
| m | mass [g] | fi | final |
| M _m | maximum weight gained [%] | i | inlet |
| N1-N15 | experimental tests | in | initial |
| P | pressure [Pa] | o | outlet |
| P _L | accumulated latent energy performance [-] | w | water |
| PM | permeability [m^2/s] | <i>Acronyms</i> | |
| \dot{Q}_L | latent thermal power [W] | AHU | air handling unit |
| R | volumetric adsorption rate [$\text{g}/\text{s m}^3$] | AM | additive manufacturing |
| Ra | arithmetic mean deviation of roughness profile [μm] | DOE | design of experiments |
| Rq | root mean square of the roughness profile [μm] | DS | desiccant system |
| Rz | maximum height of roughness profile [μm] | FC | flow conditioner |
| S | thermodynamic solubility [g/g] | FFF | fused filament fabrication |
| t | time [s] | HVAC | heating, ventilation and air conditioning |
| T | dry bulb temperature [$^\circ\text{C}$] | OP | olive pit |
| T _d | dew point temperature [$^\circ\text{C}$] | PLA | polylactic acid |
| V | volume [m^3] | PT | pitot tube |
| \dot{V} | volumetric air flow rate [m^3/s] | PW | pine wood |
| \dot{W} | electric energy consumption [W] | | |
| X | input variable | | |

these works.

In addition to the composition of desiccant materials, their physical characteristics, such as porosity, surface area or density, are crucial to increase moisture adsorption [21,22]. Porosity is a very important property that affects the adsorption capacity of materials, since desiccant dehumidification method is based on the principle of moisture adsorption into porous desiccant material [23]. The size, volume and distribution of pores significantly influenced the mass transfer between the material and the water vapor [24], since a high number of pores increases the contact area between the desiccant and the air flow. Density is another important factor in desiccant systems. Silica gel and durian peels had higher density than coconut coir, adsorbing water vapor from the air at the intermediate surface was more difficult [25]. Surface treatments can also influence the water vapor adsorption capacity of desiccant materials. For example, the surface treatment of composite materials of bamboo wood and PVC increased the water resistance of the material [26].

One of the main drawbacks of desiccant dehumidification systems is their manufacturing cost compared to conventional dehumidification systems based on direct expansion units [27]. Desiccant dehumidification systems have been manufactured for years using conventional processes, without major changes in designs or materials used. However, new paradigms such as industry 4.0, lean manufacturing and the circular economy allow and force the search for new approaches in the manufacture of these systems [28]. One of the manufacturing techniques associated with industry 4.0 is additive manufacturing (AM), also known as 3D printing, which allows a custom manufacturing process [29,30]. AM makes it possible to obtain very complex designs that are difficult to achieve through other conventional manufacturing processes [30,31]. Moreover, previous works have shown that the AM technique can be a suitable alternative for the manufacture of adsorbent materials and guarantee the optimization of energy efficiency [32]. This manufacturing technique could solve problems created by the use of

materials produced through other techniques, such as pressure drop issues.

Recently, several authors have studied the energy behaviour of heat exchanger developed using 3D printing techniques [33,34]. Two heat exchangers with a solid core of counterflow channels sandwiched between plenums were designed, manufactured through 3D printing and experimentally tested [35]. The developed systems showed excellent thermo-hydraulic performance compared to that obtained with a conventional heat exchanger. A polymeric heat exchanger with a lung-inspired design was manufactured using 3D printing [36]. High values of thermal conductivity and effectiveness were obtained for the manufactured exchanger. These authors also developed a silica gel coated heat exchanger [37], showing high volumetric adsorption rate values. However, the desiccant material coating technique could generate heterogeneous surfaces, mainly inside the channels and with complex designs, achieving a variable energy behaviour. Other authors designed and evaluated two 3D printed aircraft aluminium heat exchangers [38]. The two heat exchangers improved heat transfer compared to that of a traditionally manufactured heat exchanger, but the air side pressure drop was doubled. Thermal performance in additively manufactured metallic heat exchangers was also investigated [39], showing that complex channel designs did not necessarily obtain better energy efficiencies.

The authors of the present work have not found research studies of desiccant dehumidification systems manufactured using fused filament fabrication (FFF) 3D printing. Therefore, FFF 3D printing technology could offer new pathways for the design and manufacture of compact and efficient desiccant dehumidification systems. Investigations of air dehumidification systems developed from green desiccant materials have also not been found. The use of by-products of human activities, such as the agricultural industry, to convert them into desiccant materials could also be a great opportunity to reduce the large amount of waste generated. The main objective of this work was to develop and

experimentally evaluate the energy performance of a FFF 3D printed desiccant system using biomass-based materials. Hence, the adsorbent properties of three biodegradable materials of organic origin have been studied: polylactic acid (PLA), pine wood with PLA (PW-PLA) and olive pit with PLA (OP-PLA). After selecting the material with the best adsorbent properties, a fixed bed desiccant system has been designed, manufactured, and evaluated.

2. Methodology

2.1. Production and characterization of 3D printed desiccant materials

Three biodegradable materials of organic origin have been studied in the present work: polylactic acid (PLA), pine wood with polylactic acid (PW-PLA) and olive pit with polylactic acid (OP-PLA). PLA is the most used material in additive manufacturing; in addition, it is a hydrophilic material, for this reason it was included in this study. PLA is a thermoplastic of organic origin, which is made from corn cobs or sugar cane. Moreover, this material has several advantages, such as biodegradability and ease of extrusion [40]. The other materials are composites that were produced from PLA (80 wt%) and small particles of PW (20 wt%) or OP (20 wt%), in order to improve their desiccant capabilities. These materials also are biodegradable and compostable. PW and OP were selected due to their great presence in southern Europe.

The production process of the filaments was as follows: (i) selection of the base material: PLA; (ii) selection of organic waste: PW or OP; (iii) compounding: pellets of the mixture of raw materials; (iv) production: filament extrusion. The mixture of these compounds modified the mechanical and thermal properties of the materials. The mechanical and thermal properties of three printed specimens were obtained under different test standards and are summarized in Table 1. The crystallization temperature and melting temperature were obtained from differential scanning calorimetry tests, in order to analyse the thermal transitions of the materials when they are heated.

2.1.1. Water adsorption

The water adsorption of the three materials was analysed. The relative rate of water absorption by plastics when immersed, was tested following ISO 62 standard [41]. Three specimens were designed and manufactured for each material in the shape of a disc, as shown in Fig. 1, with a linear filling pattern and a 100% infill percentage. The specimens had a diameter of 50.8 mm and a thickness of 3.2 mm. The initial weights of the specimens were 7.66 g for PLA, 6.72 g for PW-PLA, and 6.91 g for OP-PLA. The printer used to manufacture the test specimens was the Creality Ender 3. The layer height and print temperature used to develop the specimens were 0.3 mm and 210 °C, respectively.

The specimens were dried in an oven at 50 °C for 24 h. Then they were immersed in distilled water at 23 °C for 24 h. Finally, the surface water was removed from the test specimens and weighed to the nearest 1 mg. The percentage of mass gain (Δm) over time, resulting from water adsorption, was determined using Eq. (1).

Table 1
Mechanical and thermal properties of selected materials.

| Material composition | Test standard | PLA | PW-PLA | OP-PLA |
|----------------------------------|---------------|---------|--------|---------|
| Density [g/cm ³] | ISO 1183-1 | 1.24 | 1.09 | 1.11 |
| Tensile strength [MPa] | ISO 527 | 50.00 | 32.40 | 35.80 |
| Tensile modulus [MPa] | ISO 527 | 3500.00 | 2944 | 2771.00 |
| Flexural strength [MPa] | ISO 178 | 83.00 | 65.20 | 71.60 |
| Flexural modulus [MPa] | ISO 178 | 3800.00 | 3304 | 3102.00 |
| Elongation at break [%] | ISO 178 | 6.00 | 1.20 | 1.50 |
| Hardness [Shore D] | ISO 7619-1 | 97.00 | 85.20 | 82.00 |
| Crystallization temperature [°C] | ISO 11,357 | 116.5 | 137.3 | 135.2 |
| Melting temperature [°C] | ISO 11,357 | 149.8 | 152.2 | 182.4 |

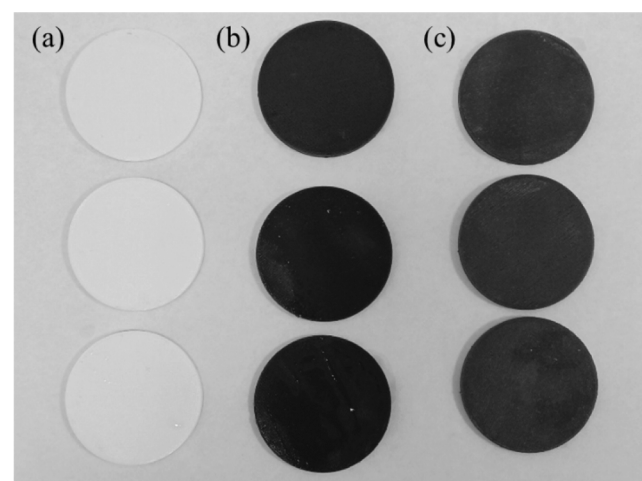


Fig. 1. Specimens of (a) PLA, (b) PW-PLA and (c) OP-PLA for the water adsorption tests.

Seasonal water adsorption was also analysed for these specimens. The specimens were studied immersed in water for 45 days (1080 h), in order to know the saturation point and if material degradation occurred.

$$\Delta m = \frac{m_f - m_{in}}{m_{in}} \cdot 100 \quad (1)$$

Diffusion is one of the main mechanisms of water adsorption of materials composed of polymers with organic materials. Diffusion shows the ability of water molecules to penetrate inside the materials. The diffusion coefficients (D) have been obtained for the three materials, calculated with Eq. (2), [42].

$$D = \pi \cdot \left(\frac{b \cdot \theta}{4 \cdot M_m} \right)^2 \quad (2)$$

where b is the thickness of the composite (m); θ is the initial slope of a plot of $M(t)$ versus $t^{1/2}$; and M_m is the maximum weight gained (%).

The parameters of thermodynamic solubility (S) and permeability (PM) of the three materials have also been obtained with Eqs. (3) and (4), respectively. The solubility is related to the increase in mass of water (Δm), while the permeability parameter is defined as the product of the diffusion coefficient and the solubility [42].

$$S = \frac{m_w}{m_{in}} \quad (3)$$

$$PM = D \cdot S \quad (4)$$

where m_w is the mass of adsorbed water in the equilibrium state and m_{in} is the initial mass of the material sheet.

2.1.2. Moisture adsorption tests and material selection

For measuring the sorption properties of the materials, on the one hand, water vapor adsorption and desorption isotherms were determinate to know the amount of moisture adsorbed by each material under different relative pressures. These tests were carried out at 298 K. On the other hand, nitrogen adsorption and desorption isotherms were carried out at 77 K to measure the surface area, pore size and pore volume. A Micromeritics 3Flex Surface Characterization system was used to obtain these sorption isotherms. These results were used to select the best material to print the prototype.

2.2. Design and manufacture of the desiccant system

A fixed bed desiccant system was designed using the material with the highest adsorption capacity, see Fig. 2. Two similar modules of this

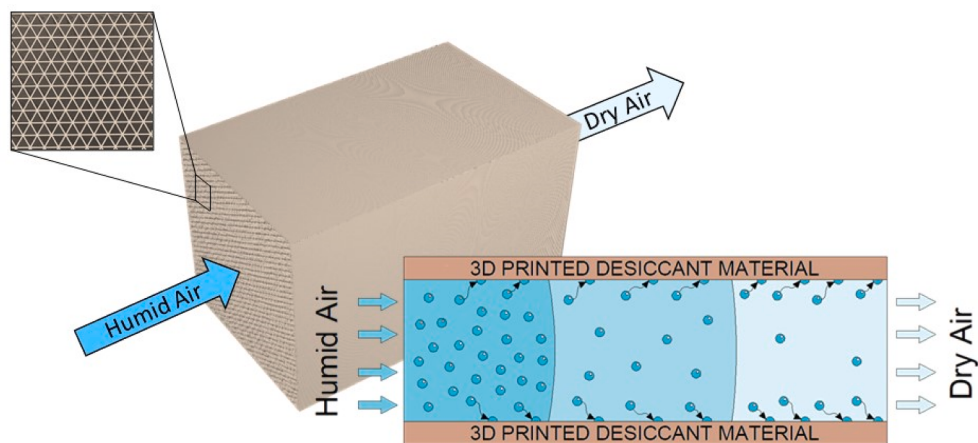


Fig. 2. Schematic of the desiccant system layout and air circulation channels.

desiccant system will be necessary to have a continuous dehumidification process, given its fixed bed design. That is, one module will be used to dehumidify air and another module to regenerate the material. The dimensions of the desiccant system were $100 \times 100 \times 150 \text{ mm}^3$ (width, height and length). The prototype was designed using SolidWorks software [43] and exported to Ultimaker Cura software [44] for subsequent slicing and printing. The printing parameters used to manufacture the desiccant system were: layer height of 0.3 mm; infill of 45%; print speed of 50 mm/s; print temperature of 210 °C; hot pad of 50 °C; and fan layer of 100 %. The desiccant element geometry is shown in Fig. 2. The shape and size of the channels have a significant impact on the heat and mass transfer process [45,46]. In the present work, channels with an

equilateral triangular shape were chosen, with side length of 2 mm. The thickness of the walls between adjacent channels was of 0.5 mm.

2.3. Experimental energy performance of the desiccant system

The developed desiccant system was experimentally analysed under different air conditions. An experimental setup was used for this analysis, see Fig. 3. The air inlet conditions to the system were controlled with an air handling unit (AHU), see Fig. 3a. AHU was mainly composed of a heating coil, a cooling coil, a steam humidifier, and a variable speed fan. Flow conditioners have also been installed at the facility to achieve uniform airflow conditions and a pitot tube to measure the inlet airflow

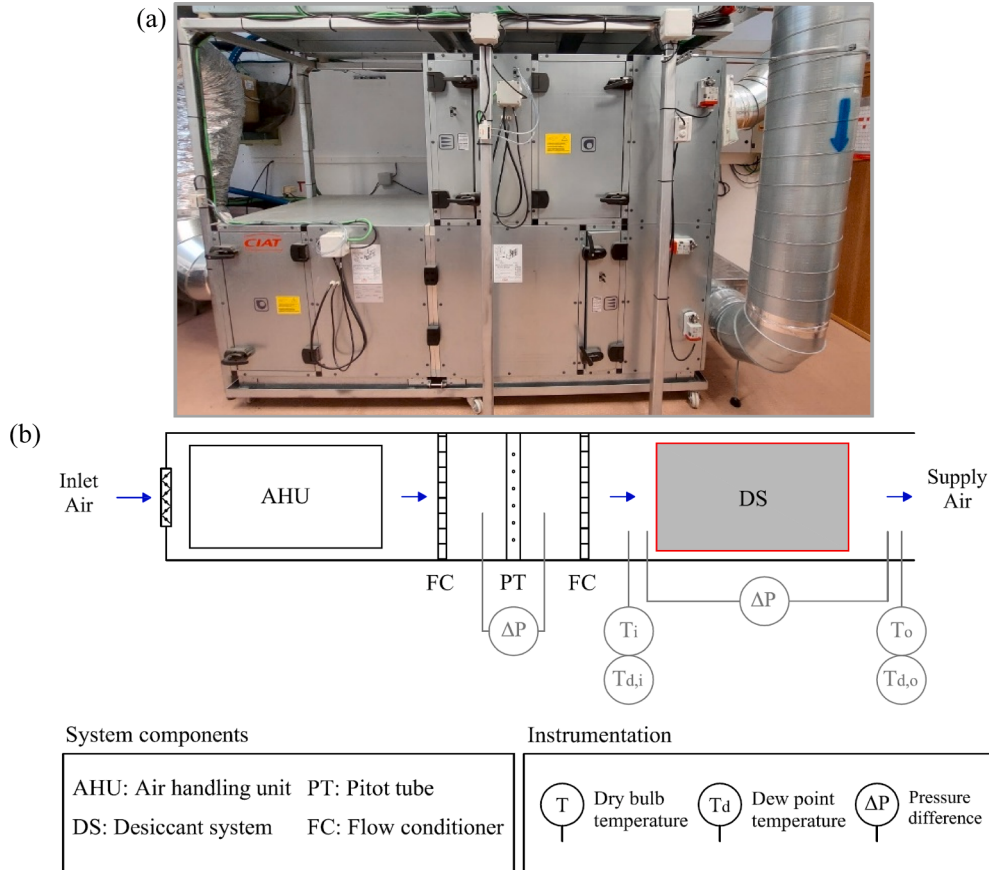


Fig. 3. (a) An image of the air handling unit; (b) schematic of the experimental setup.

rate. The dry bulb temperature (T) and dew point temperature (T_d) were measured at the inlet and outlet of the desiccant system, as well as the pressure drop (ΔP) of the system, see Fig. 3b. The technical specifications of the measuring devices are shown in Table 2. All the experimental tests were carried out under steady state conditions, with sampling time of 3 s.

The statistical technique of design of experiments (DOE) was used to analyse the desiccant system, with a Box-Behnken design. The input variables were inlet air flow rate (\dot{V}_i), inlet dry bulb temperature (T_i) and inlet dew point temperature ($T_{d,i}$). The ranges of the variables were from $50 \text{ m}^3/\text{h}$ to $150 \text{ m}^3/\text{h}$ for \dot{V}_i , from 24°C to 40°C for T_i and from 10°C to 20°C for $T_{d,i}$. The inlet air conditions were selected to test the prototype under a wide range of inlet air temperature, air humidity, and air flow. The values of these ranges correspond to mild and warm climatic conditions. The inlet regeneration air conditions were always set constant: $T_i = 50^\circ\text{C}$ and $T_{d,i} = 10^\circ\text{C}$. Low regeneration air temperature was used in the desiccant system to be able to integrate it with renewable energy systems, thus reducing the environmental impact associated with air dehumidification. The output variables of the DOE were accumulated moisture removal capacity (MRC_a), Eq. (8), and accumulated latent energy performance (P_L), Eq. (9). The values of MRC_a and P_L were obtained for a dehumidification period of 300 s. The set of experimental tests of the desiccant system was summarized in Table 3. Moreover, the desirability function was used to obtain the optimal value of multiple responses (MRC_a and P_L). This function is a solution to combine the responses of multiple factors into a single function.

The energy performance of the developed desiccant system was evaluated according to the following parameters:

- Variation of air humidity ratio ($\Delta\omega$) and pressure drop (ΔP) of the desiccant system.

$$\Delta\omega = \omega_i - \omega_o \quad (5)$$

$$\Delta P = P_i - P_o \quad (6)$$

- Instantaneous moisture removal capacity (MRC). Where \dot{m}_i is inlet mass air flow rate.

$$MRC = \dot{m}_i \cdot (\omega_i - \omega_o) \quad (7)$$

- Accumulated moisture removal capacity (MRC_a) during a dehumidification period of 300 s.

$$MRC_a = \frac{\dot{m}_i}{\Delta t} \int_0^t (\omega_i - \omega_o) dt \quad (8)$$

- Accumulated latent energy performance (P_L) during a dehumidification period of 300 s. Where \dot{Q}_L is latent thermal power, calculated with Eq. (10), and \dot{W}_f is electric energy consumption of the fan, calculated with Eq. (11), considering a fan efficiency (η_f) of 0.5.

$$P_L = \frac{\int_0^t \dot{Q}_L dt}{\int_0^t \dot{W}_f dt} \quad (9)$$

$$\dot{Q}_L = \dot{m}_i \cdot (\omega_i - \omega_o) \cdot \Delta h_{vap} \quad (10)$$

Table 2
Technical specification of measuring devices.

| Parameter | Type of sensor | Accuracy |
|------------|-----------------------------------|--------------------------|
| T | PT100 | $\pm 0.20^\circ\text{C}$ |
| Td | Chilled mirror hygrometer | $\pm 0.15^\circ\text{C}$ |
| ΔP | Differential pressure transmitter | $\pm 5.00 \%$ |

Table 3
Experimental tests of the desiccant system.

| N | $\dot{V}_i [\text{m}^3/\text{h}]$ | $T_i [^\circ\text{C}]$ | $T_{d,i} [^\circ\text{C}]$ |
|----|-----------------------------------|------------------------|----------------------------|
| 1 | 50 | 32 | 10 |
| 2 | 100 | 24 | 10 |
| 3 | 100 | 40 | 10 |
| 4 | 150 | 32 | 10 |
| 5 | 50 | 24 | 15 |
| 6 | 50 | 40 | 15 |
| 7 | 100 | 32 | 15 |
| 8 | 100 | 32 | 15 |
| 9 | 100 | 32 | 15 |
| 10 | 150 | 24 | 15 |
| 11 | 150 | 40 | 15 |
| 12 | 50 | 32 | 20 |
| 13 | 100 | 24 | 20 |
| 14 | 100 | 40 | 20 |
| 15 | 150 | 32 | 20 |

$$\dot{W}_f = \frac{\Delta P \cdot \dot{V}_i}{\eta_f} \quad (11)$$

- Volumetric adsorption rate (R) calculated with MRC_a and total volume (V) of the desiccant system.

$$R = \frac{MRC_a}{V} \quad (12)$$

3. Results and discussion

3.1. Material analysis

The water and humidity adsorption capacity for each material (PLA, PW-PLA and OP-PLA) were evaluated in this section.

3.1.1. Water adsorption capacity

The water adsorption for the selected materials was analysed. The results of the samples for each material are shown in Fig. 4. The water adsorption capacity, Δm , was determined from Eq. (1). It can be observed that the material with the highest water adsorption at 24 h was PW-PLA, with values between 4.4 % and 4.8 %. The Δm values for the samples of PLA and the samples of OP-PLA were significantly lower than those achieved with PW-PLA. The Δm values of PLA were between 2% and 1.75% and the Δm values of OP-PLA were between 2.2% and 2.6%.

The seasonal water adsorption capacity of these samples was also analysed. The samples were immersed in water for 1080 h (45 days). The

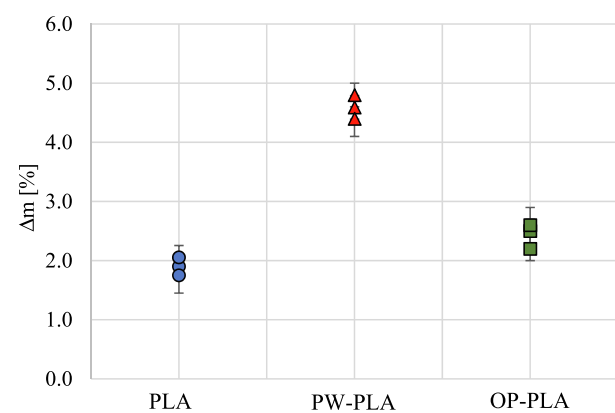


Fig. 4. Water adsorption at 24 h for the selected materials: PLA, PW-PLA and OP-PLA.

measured Δm values of the three samples of each material are shown in Fig. 5. The results of the samples of PW-PLA and OP-PLA followed increasing trends throughout the period, up to 11.4 % and 7.0 %, respectively. Therefore, the tests of the samples of PW-PLA and OP-PLA showed that these materials did not deteriorate during the period studied. However, the results of the samples of PLA achieved a maximum value of 2.6 % at 72 h, decreasing its value from that period.

These results show the use of green desiccant materials based on natural resources, such as pine wood or olive pit, could have a positive environmental impact in the production of new desiccant systems. Previous research works have also analysed the water adsorption capacity of materials composed of polymers and agricultural waste [47]. Pujari et al. [48] studied the maximum water adsorption capacity of a material composed of polyester and jute fibres (20, 40, 60, 100 vol%), reaching values between 5.7 % and 14 %. Robledo-Ortíz et al. [49] showed that materials composed of polyethylene and agave (20 and 30 wt%) reached maximum values of water adsorption capacity of 11.7–20 %. A recycled blend of HDPE/PET with rice husk (40, 60 and 80 wt%) was analysed by Chen et al. [50], reaching maximum water adsorption capacity values of 6.2–14.7 %. Based on previous results, the water adsorption capacity of the analysed materials could increase if the content of pine wood or olive pit is increased.

Once the maximum water adsorption capacity was known, the diffusion coefficient (D), thermodynamic solubility (S) and permeability (PM) were obtained. The results of D, S and PM for the three materials are shown in Table 4. These results showed that water molecules diffuse more easily in PLA and PW-PLA than in OP-PLA, that is, the diffusion process was faster. In addition, PW-PLA was the material that had the highest values of solubility and permeability to water.

3.1.2. Moisture adsorption capacity

The adsorption capacity of the three materials were measured through adsorption–desorption isotherms, as shown in Fig. 6. The trends of the sorption curves were similar for the three materials, with a visible hysteresis occurring. These results show that PW-PLA was the material with the highest adsorption capacity, 82% more than PLA and 12.7% more than OP for a relative pressure of 0.8. Therefore, the presence of PW or OP significantly improved the adsorption capacity, however it was limited due to the high percentage of PLA (80 wt%).

The water adsorption capacity of a material depends on its structure, composition and surface. Previous works have proven that the surface and porosity of the materials are very influential properties in the adsorption capacity [16]. The surface characteristics of PW-PLA and OP-

Table 4

Results of diffusion coefficient, solubility and permeability for the three materials.

| Material | D [m^2/s] | S [g/g] | PM [m^2/s] |
|----------|----------------------|---------|-----------------------|
| PLA | $6.61 \cdot 10^{-9}$ | 0.019 | $1.29 \cdot 10^{-10}$ |
| PW-PLA | $3.25 \cdot 10^{-9}$ | 0.118 | $3.82 \cdot 10^{-10}$ |
| OP-PLA | $1.77 \cdot 10^{-9}$ | 0.081 | $1.44 \cdot 10^{-10}$ |

PLA were obtained from nitrogen adsorption and desorption isotherm tests. These tests allowed to determine the specific surface area, pore volume and pore size, as shown in Table 5. It can be observed than PW-PLA was the material with the largest surface area, $0.1213\text{ m}^2/\text{g}$, so it is the most porous material. PW-PLA also had the highest volume values for adsorption pore widths less than 403.122 \AA and for desorption pore widths less than 25.859 \AA . The average pore diameter of both materials did not vary significantly. These results suggest that the higher porosity of PW-PLA helped to improve its adsorption capacity compared to OP-PLA.

3.2. Evaluation of the performance of the manufactured desiccant system

A desiccant dehumidification prototype was manufactured with the material selected in section 3.1, PW-PLA, and using the FFF 3D printing technique. An image of the 3D printed green desiccant system is shown in Fig. 7. It can be seen a good manufacturing accuracy of the prototype channels. The dimensions of the manufactured prototype are summarized in Section 2.2.

3.2.1. Thermal behaviour analysis

For the manufactured desiccant system, the variation of air humidity ratio, $\Delta\omega$, and moisture removal capacity, MRC, during the dehumidification process was analysed for different experimental tests. The tests N1, N4, N12 and N15 of Table 3 were used for this study, as shown in Fig. 8. The inlet air temperature was constant in all these tests, 32°C . It can be observed that the maximum $\Delta\omega$ values were achieved at the beginning of the dehumidification process, see Fig. 8a. The air dehumidification was due to the water vapor pressure difference between the air and the desiccant material. The $\Delta\omega$ values decreased with time, so the difference in water vapor pressure between the material and the air was reduced, and consequently its desiccant capacity was also reduced. This trend was coherent with the results obtained by the authors in previous work on desiccant wheels [51].

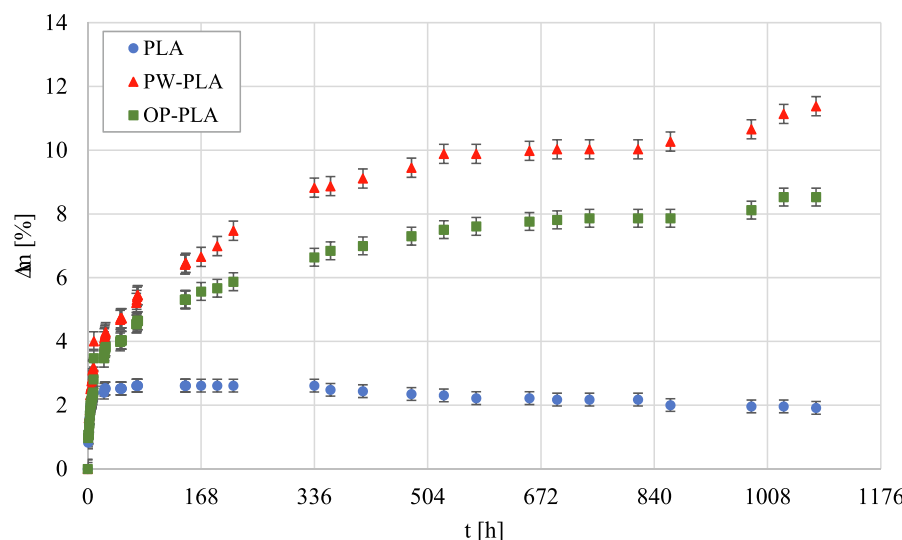


Fig. 5. Experimental sorption curves for the selected materials: PLA, PW-PLA and OP-PLA.

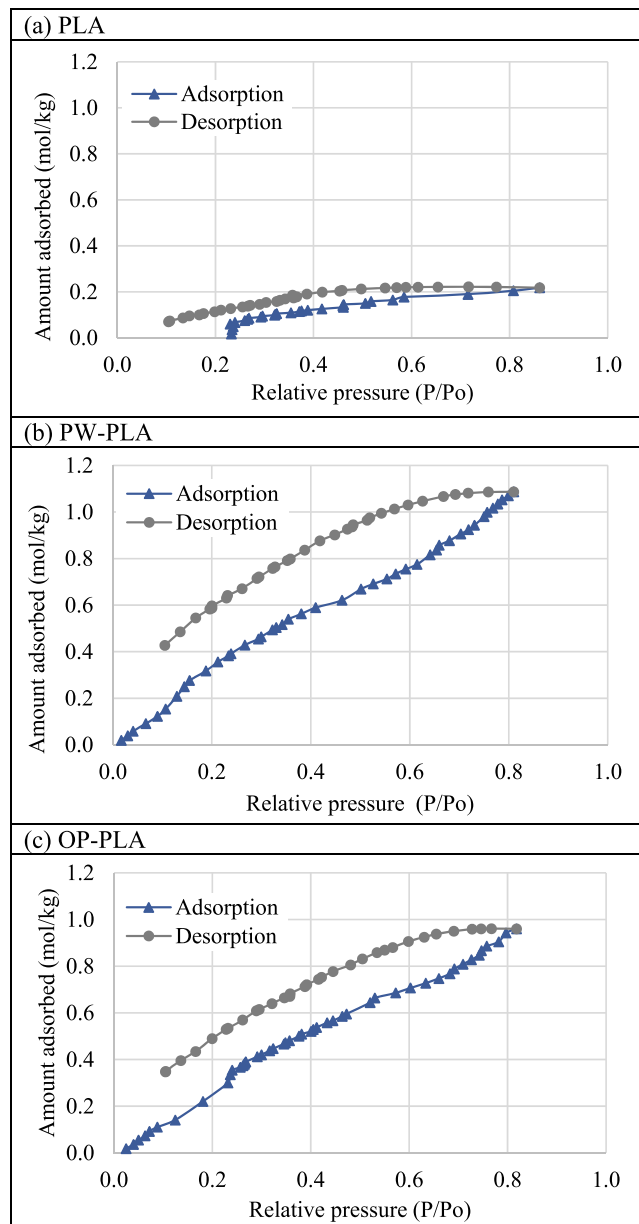


Fig. 6. Water vapor adsorption and desorption isotherms for the selected materials: PLA, PW-PLA and OP-PLA.

Table 5
Surface properties of PW-PLA and OP-PLA.

| Material | PW-PLA | OP-PLA |
|---|----------|----------|
| Surface Area | | |
| BET Surface área [m ² /g] | 0.1213 | 0.0418 |
| Pore Volume | | |
| Single point adsorption total pore volume of pores less than 403.122 Å width at P/Po = 0.950000000 [cm ³ /g] | 0.000174 | 0.000083 |
| Single point desorption total pore volume of pores less than 25.859 Å width at P/Po = 0.300056319 [cm ³ /g] | 0.000049 | 0.000017 |
| Pore Size | | |
| Adsorption average pore diameter [Å] | 57.391 | 79.634 |
| Desorption average pore diameter [Å] | 16.113 | 16.288 |

The experimental results of these case studies also showed that $\Delta\omega$ was higher, the higher $T_{d,i}$, as expected, see N12 versus N1 and N15 versus N4 (Fig. 8a). The initial $\Delta\omega$ values were similar when $T_{d,i}$ and T_i

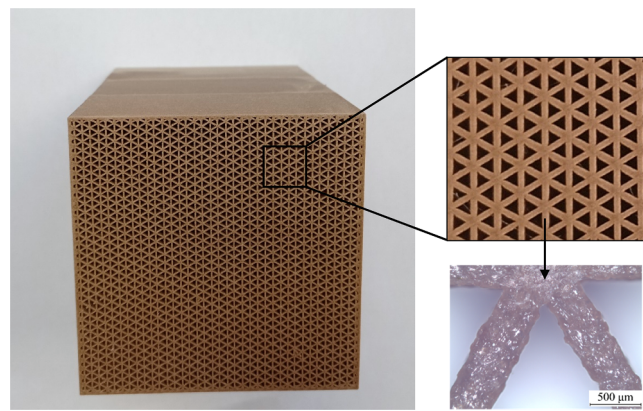


Fig. 7. Images of the 3D printed green desiccant system using PW-PLA and of the air channels. (For interpretation of the references to colour in this figure legend, the reader is referred to the web version of this article.)

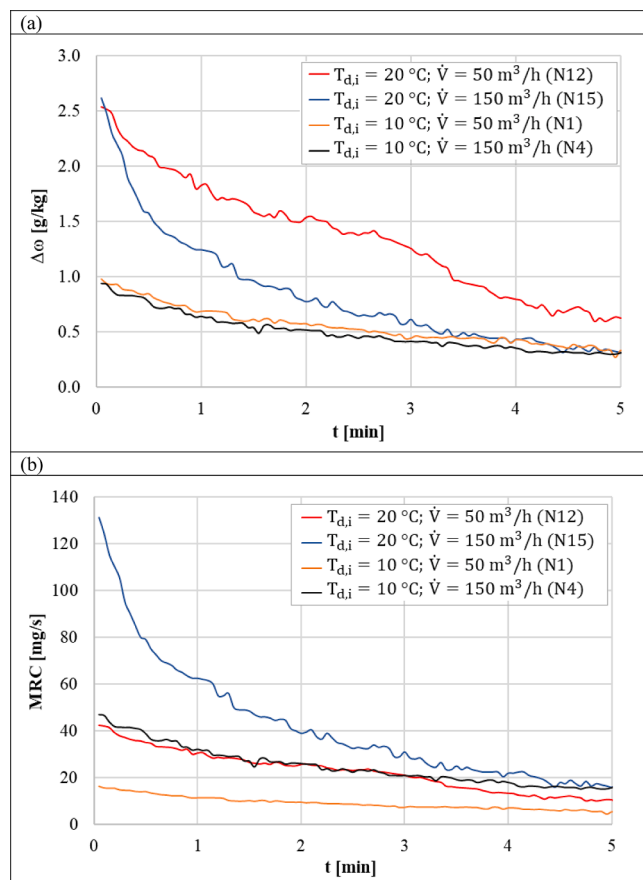


Fig. 8. Variation of (a) $\Delta\omega$ and (b) MRC for different values of $T_{d,i}$ and \dot{V} during the dehumidification process using the 3D printed green desiccant system. (For interpretation of the references to colour in this figure legend, the reader is referred to the web version of this article.)

were constant, as shown in the case studies N12-N15 (approximately 2.6 g/kg) and N1-N4 (approximately 0.95 g/kg), see Fig. 8a, since the water vapor pressure difference at the beginning was similar in these cases. However, the evolution of $\Delta\omega$ during the dehumidification process varied for each case. The higher the air flow rate, the higher the reduction in $\Delta\omega$. For high $T_{d,i}$ values (N12 and N15), this reduction in $\Delta\omega$ was higher than that for low $T_{d,i}$ values (N1 and N4). This variation was due to the fact that the mass transfer from the air to the desiccant material was greater for high air flow rates, increasing the rate of moisture

adsorption. Similar behaviour was obtained in previous research works [37].

The MRC values were also obtained for these case studies, see Fig. 8b. This parameter is directly related to $\Delta\omega$ and \dot{V} , as shown in Eq. (7). Therefore, the higher $\Delta\omega$ and \dot{V} , the higher the MRC value. The highest MRC value was 131 mg/s, obtained at the beginning of the dehumidification process of test N15. The MRC value decreased significantly over time, with reductions of 52.7% after one minute of the dehumidification process, up to 62 mg/s, and 70.2% after two minutes, up to 39 mg/s. Therefore, these results suggest that the time of the dehumidification process should be controlled in order not to significantly reduce the desiccant capacity of this system.

The pressure drop, ΔP , of the desiccant system was measured for different inlet air flow rates, from 20 m³/h to 170 m³/h, see Fig. 9. It can be seen that the experimental ΔP results followed an exponential trend, varied from 100 Pa to 730 Pa. Moreover, these ΔP values were used to calculate the electric energy consumption of a fan, \dot{W}_f , see Fig. 9. The \dot{W}_f values ranged between 2.5 W and 69.9 W.

If a desiccant system application requires a higher air flow rate than used in this system, the cross-sectional area (width and height) of the system should be increased proportionally. In this way, the moisture removal capacity would also be increased, keeping pressure drop constant.

3.2.2. Statistical analysis

The statistical technique of Design of Experiments (DOE) was used to analyse accumulated moisture removal capacity (MRC_a) and accumulated latent energy performance (P_L) of the dehumidification system. The values of MRC_a and P_L were obtained for a dehumidification period of 300 s. The results of the ANOVA for MRC_a and P_L are summarized in Table 6. This table shows each of the main estimated effects, the standard error of each of the effects, the statistical parameter F-Ratio and the statistical parameter P-value, which is used as a tool to check the significance of each effect. It can be observed that the three input variables were found significant at 95% confidence level, since the P-values were lower than 0.05 in all cases. The most influential input variables on MRC_a and P_L , from highest to lowest, were: \dot{V} , $T_{d,i}$ and T_i . Therefore, the inlet airflow rate should be controlled to adjust the adsorption capacity and performance of the desiccant system. The models of MRC_a and P_L were found to be suitable for the observed data at 95% confidence level, as the P-values for lack-of-fit tests were greater than 0.05 in all cases, see Table 6. The R^2 value for MRC_a and P_L were always greater than 95%, so the prediction of these parameters is in agreement with the experimental results.

Simplified empirical models of MRC_a and P_L for the dehumidification system was also obtained using the DOE methodology. The relationship

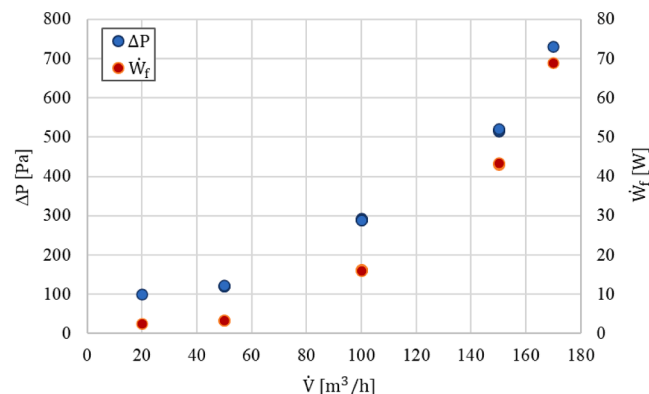


Fig. 9. Pressure drop and electric energy consumption of the fan of the 3D printed green desiccant system. (For interpretation of the references to colour in this figure legend, the reader is referred to the web version of this article.)

between the output parameters and input variables was adjusted using second order polynomial equations, expressed by Eq. (13). Where \hat{Y} was the estimated output value (MRC_a and P_L), X_i were linear variables, quadratic variables or their interactions and a_i and a_{ii} were the estimated coefficients summarized in Table 7. These mathematical models would also be valid for other desiccant systems made with the same material, the same channel dimensions, and the same cross-sectional area – airflow ratio. Therefore, the models allow analysing desiccant systems with different volumes and applications.

$$\hat{Y} = a_0 + \sum_{i=1}^k a_i \cdot X_i + \sum_{i=1}^k a_{ii} \cdot X_i^2 \quad (13)$$

3.2.3. Moisture removal capacity and latent coefficient of performance

The relationship between the output parameters, MRC_a and P_L , and the input variables most influential input variables found in Table 6 (\dot{V} and $T_{d,i}$) were analysed, see Fig. 10. For these case studies, T_i was fixed at constant value, 32 °C. It can be observed that the maximum MRC_a value was 39 mg/s, achieved for the highest values of \dot{V} and $T_{d,i}$ and during a dehumidification period of 300 s, see Fig. 10a. On the contrary, the minimum MRC_a value was 11 mg/s, obtained for the lowest values of \dot{V} and $T_{d,i}$ and during a dehumidification period of 300 s. Therefore, the desiccant capacity of the manufactured system increased for moist inlet air conditions. Regarding P_L , it can be seen that it increased when the \dot{V} value decreased, see Fig. 10b. For low \dot{V} , the pressure drop was reduced and consequently, the electrical energy consumption of the fan was reduced, as shown in Fig. 9. The P_L values were also improved when the $T_{d,i}$ values increased, mainly due to increased desiccant capacity under humid conditions. The maximum P_L value was 16.5 for values of \dot{V} and $T_{d,i}$ of 50 m³/h and 20 °C, respectively. The results showed that high values of MRC_a and P_L can be achieved with the system developed from additive manufacturing and using PW-PLA.

Evaluating optimal results of MRC_a and P_L , it can be seen that the maximum values of these output parameters were found for different \dot{V} values, as shown in Fig. 10. Therefore, the desirability function was used in order to maximize both parameters, see Fig. 11. This function allowed to determine the combination of experimental factors that simultaneously optimize several response parameters. For this case study, the optimum desirability value was 0.77, obtained for the minimum \dot{V} value, 50 m³/h, and the maximum $T_{d,i}$ value, 20 °C. The values of MRC_a and P_L corresponding to the optimal desirability value were 26 mg/s and 16.5, respectively, for a dehumidification period of 300 s.

3.2.4. Comparative analysis

The results of the manufactured dehumidification system have been compared with those of other desiccant heat exchangers studied in the literature. The volumetric adsorption rate, R , and the pressure drop, ΔP , of the system were calculated for all experimental tests, Table 3. These results were represented in Fig. 12. For the present work, the R values varied from 6.4 g/s·m³ to 30 g/s·m³ for ΔP of 120 Pa and 522 Pa, respectively, during a dehumidification period of 300 s. If the dehumidification period had been less than the current one, the R values would increase, as shown in Fig. 8. A desiccant coated heat exchanger inspired by the lungs was analysed by Puttur et al [37], reaching higher R values than those obtained in the present work, up to 54.8 g/s·m³. However, the pressure drop value was significantly higher, 4000 Pa. A desiccant heat exchanger packed with silica gel was developed and analysed by Mohammed et al. [23]. The R value was similar to that achieved in the present work, 22 g/s·m³, but with much higher pressure drop, 1000 Pa, and the dehumidification period was shorter, 3.3 min. The three desiccant systems were regenerated at 50 °C. Therefore, the 3D printed desiccant dehumidification system reached adequate R values with low pressure drop compared to previous systems studied.

Table 6

Effects of input variables on output variables of the desiccant system.

| Effect | MRC _a | | | | P _L | | | |
|------------------|--------------------------|-------------|---------|---------|--------------------------|-------------|---------|---------|
| | Estimate | Stnd. Error | F-Ratio | P-value | Estimate | Stnd. Error | F-Ratio | P-value |
| Average | 20.20 | 0.47 | | | 3.42 | 0.25 | | |
| \dot{V} | 13.79 | 0.57 | 582.3 | 0.0017 | -10.98 | 0.30 | 1333.4 | 0.0007 |
| T _i | -2.50 | 0.57 | 19.2 | 0.0400 | -1.25 | 0.30 | 18.4 | 0.0430 |
| T _{d,i} | 12.74 | 0.57 | 496.8 | 0.0020 | 3.82 | 0.30 | 202.5 | 0.0061 |
| Lack-of-fit | | | 19.09 | 0.0502 | | | 16.67 | 0.0571 |
| | R ² : 95.29 % | | | | R ² : 96.99 % | | | |

Table 7Estimated coefficients of the empirical models of MRC_a and P_L.

| Estimated coefficients | X _i | MRC _a × 10 ⁻³ [mg/s] | P _L × 10 ⁻³ [-] |
|------------------------|-----------------------------------|--|---------------------------------------|
| a ₀ | - | 28550.00 | 18458.70 |
| a ₁ | \dot{V} | -71.56 | -307.72 |
| a ₂ | T _i | -34.01 | -322.55 |
| a ₃ | T _{d,i} | -2424.00 | 1252.75 |
| a ₄ | \dot{V}^2 | 0.82 | 1.26 |
| a ₅ | $\dot{V} \cdot T_i$ | 3.35 | 2.93 |
| a ₆ | $\dot{V} \cdot T_{d,i}$ | -4.07 | -9.81 |
| a ₇ | T _i ² | -8.57 | -0.96 |
| a ₈ | T _i · T _{d,i} | 6.06 | 0.88 |
| a ₉ | T _{d,i} ² | 130.37 | 2.73 |

4. Conclusions

The energy performance of a 3D printed air dehumidification system using green desiccant materials was analysed. Hence, the adsorption capacity of three biomass-based materials were studied: polylactic acid (PLA), pine wood with polylactic acid (PW-PLA) and olive pit with polylactic acid (OP-PLA). The fused filament fabrication technology was used to manufacture this desiccant system.

Moisture adsorption analysis showed that the samples of PW-PLA retained higher amount of water vapor than the samples made from only PLA or OP-PLA, up to 82 % and 12.7 %, respectively, due to their composition and specific surface. Therefore, the material with PW-PLA was the most suitable for the manufacture of the desiccant dehumidification system in terms of moisture adsorption. After selecting the material, a desiccant system with a fixed bed design was manufactured. The additive manufacturing technique enabled to achieve excellent manufacturing precision of the prototype channels. The experimental evaluation of the energy performance of the desiccant system showed adequate moisture removal capacity values, up to 131 mg/s, with a low regeneration air temperature value, 50 °C. The moisture removal capacity values decreased significantly over time, so dehumidification

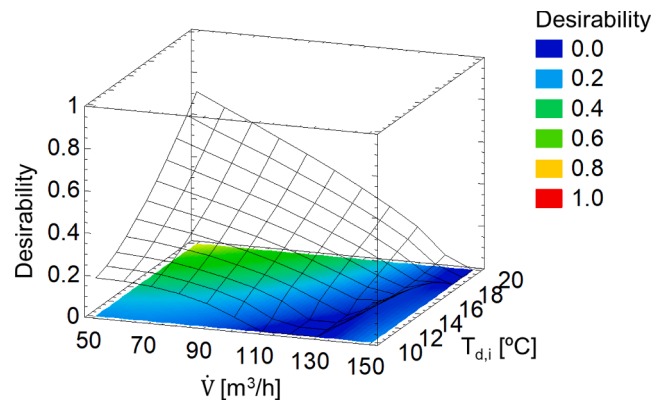


Fig. 11. Response surface optimization.

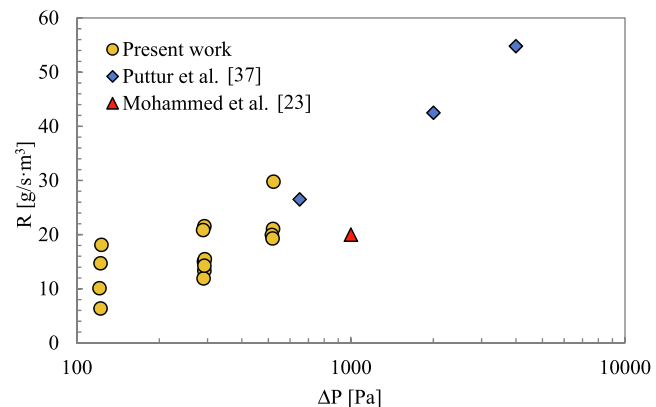
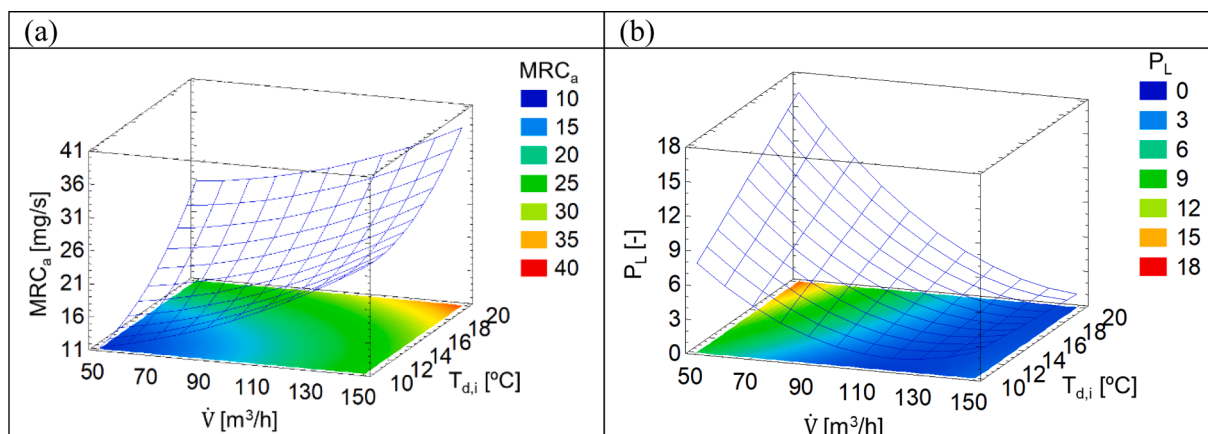


Fig. 12. Comparative analysis of volumetric adsorption rate, R, and the pressure drop, ΔP.

Fig. 10. Response surfaces of MRC_a and P_L for different values of \dot{V} and T_{d,i}.

process should be controlled in order not to significantly reduce the desiccant capacity of this system. Moreover, a comparative analysis showed that the 3D printed desiccant system reached similar volumetric adsorption rate values to previous works, up to 30 g/s m^3 , but with a lower pressure drop, less than 552 Pa. Consequently, high latent energy performance values were achieved, up to 16.5.

These results showed the promising potential of developing dehumidification systems using 3D printing and green desiccant materials, which could be an interesting ecological alternative to other desiccant systems. The manufactured system could be used in multiple applications, such as food dryers, chemical processes, or air conditioning systems. Moreover, 3D printing technology also makes it possible to develop desiccant systems with customized sizes and designs, such as a desiccant wheel.

Declaration of Competing Interest

The authors declare that they have no known competing financial interests or personal relationships that could have appeared to influence the work reported in this paper.

Data availability

Data will be made available on request.

Acknowledgement

These results are part of the project DCOOL, reference TED2021-129648B-I00, funded by MCIN/AEI/10.13039/501100011033 and the European Union "NextGenerationEU/PRTR". Recovery, Transformation and Resilience Plan - funded by the European Union - NextGenerationEU. The authors also acknowledge the financial support received by European Union's Horizon 2020 research and innovation programme, through the research project WEDISTRICT, reference H2020-WIDESPREAD2018-03-857801. The authors would also like to acknowledge Smart Materials 3D for their technical support. Funding for open access charge: Universidad de Córdoba / CBUA.

References

- [1] European Parliament, European Directive 2010/31/EU on the Energy Performance of Buildings, 2010. 10.3000/17252555.L_2010.153.eng.
- [2] J. Woods, N. James, E. Kozubal, E. Bonnema, K. Brief, L. Voeller, J. Rivest, Humidity's impact on greenhouse gas emissions from air conditioning, Joule. (2022), <https://doi.org/10.1016/j.joule.2022.02.013>.
- [3] F. Comino, M. Ruiz de Adana, F. Peci, Energy saving potential of a hybrid HVAC system with a desiccant wheel activated at low temperatures and an indirect evaporative cooler in handling air in buildings with high latent loads, Appl. Therm. Eng. 131 (2018) 412–427. [j.applthermaleng.2017.12.004](#).
- [4] O.M. Zaki, R.H. Mohammed, O. Abdelaiziz, Separate sensible and latent cooling technologies: a comprehensive review, Energy Convers. Manag. 256 (2022). [j.enconman.2022.115380](#).
- [5] L.G. Harriman III, *The Dehumidification Handbook*, second ed., Munters Corporation, Amesbury, MA, 2003.
- [6] F. Comino, D. Guijo-Rubio, M. Ruiz de Adana, C. Hervás-Martínez, Validation of multitask artificial neural networks to model desiccant wheels activated at low temperature, Int. J. Refrig. 100 (2019). [j.ijrefrig.2019.02.002](#).
- [7] I. Yaningsih, A.T. Wijayanta, T. Miyazaki, S. Koyama, Analysis of heat and mass transfer characteristics of desiccant dehumidifier system with honeycomb configuration, Appl. Therm. Eng. 144 (2018). [j.applthermaleng.2018.08.066](#).
- [8] I. Yaningsih, A.T. Wijayanta, T. Miyazaki, Heat and mass transfer characteristics of a desiccant dehumidification system operating by low regeneration temperature, Heat Transfer Eng. 43 (2022), <https://doi.org/10.1080/01457632.2021.2000582>.
- [9] J. Guo, J.I. Bilbao, A.B. Sproul, Parametric number of transfer unit analysis of a photovoltaic thermal coupled desiccant dehumidifier, Energy Convers. Manag. 255 (2022) 115339. [j.enconman.2022.115339](#).
- [10] F. Comino, J. Castillo González, F.J. Navas-Martos, M. Ruiz de Adana, Experimental energy performance assessment of a solar desiccant cooling system in Southern Europe climates, Appl. Therm. Eng. 165 (2020) 114579. [j.applthermaleng.2019.114579](#).
- [11] L.Z. Zhang, H.X. Fu, Q.R. Yang, J.C. Xu, Performance comparisons of honeycomb-type adsorbent beds (wheels) for air dehumidification with various desiccant wall materials, Energy. 65 (2014) 430–440. [j.energy.2013.11.042](#).
- [12] H. Kim, H.J. Cho, S. Narayanan, S. Yang, H. Furukawa, S. Schiffres, X. Li, Y. B. Zhang, J. Jiang, O.M. Yaghi, E.N. Wang, Characterization of adsorption enthalpy of novel water-stable zeolites and metal-organic frameworks, Sci. Rep. 6 (2016) 1–8, <https://doi.org/10.1038/srep19097>.
- [13] K.J. Chua, Heat and mass transfer of composite desiccants for energy efficient air dehumidification: Modelling and experiment, Appl. Therm. Eng. 89 (2015) 703–716. [j.applthermaleng.2015.06.061](#).
- [14] L.M. Hu, T.S. Ge, Y. Jiang, R.Z. Wang, Performance study on composite desiccant material coated fin-tube heat exchangers, Int. J. Heat Mass Transf. 90 (2015) 109–120. [j.ijheatmasstransfer.2015.06.033](#).
- [15] A. Karmakar, V. Prabakaran, D. Zhao, K.J. Chua, A review of metal-organic frameworks (MOFs) as energy-efficient desiccants for adsorption driven heat-transformation applications, Appl. Energy. 269 (2020) 115070. [j.apenergy.2020.115070](#).
- [16] N. Asim, Z. Emdadi, M. Mohammad, M.A. Yarmo, K. Sopian, Agricultural solid wastes for green desiccant applications: an overview of research achievements, opportunities and perspectives, J. Clean. Prod. 91 (2015) 26–35. [j.clepro.2014.12.015](#).
- [17] D. Sidiras, F. Batzias, E. Schroeder, R. Ranjan, M. Tsapatsis, Dye adsorption on autohydrolyzed pine sawdust in batch and fixed-bed systems, Chem. Eng. J. 171 (2011) 883–896. [j.cej.2011.04.029](#).
- [18] M. Özcar, I.A. Şengül, Adsorption of metal complex dyes from aqueous solutions by pine sawdust, Bioresour. Technol. 96 (2005) 791–795. [j.biotech.2004.07.011](#).
- [19] S. Eder, K. Müller, P. Azzari, A. Arcifa, M. Peydayesh, L. Nyström, Mass transfer mechanism and equilibrium modelling of hydroxytyrosol adsorption on olive pit-derived activated carbon, Chem. Eng. J. 404 (2021) 126519. [j.cej.2020.126519](#).
- [20] Z. Emdadi, N. Asim, M. Ambar Yarmo, M. Ebadi, M. Mohammad, K. Sopian, Chemically treated rice husk blends as green desiccant materials for industrial application, Chem. Eng. Technol. 40 (2017) 1619–1629, <https://doi.org/10.1002/ceat.201600105>.
- [21] M.D. Zaveri, Absorbency Characteristics of Kenaf Core Particles, 2004.
- [22] X.N. Wu, T.S. Ge, Y.J. Dai, R.Z. Wang, Review on substrate of solid desiccant dehumidification system, Renew. Sust. Energy Rev. 82 (2018) 3236–3249. [j.rser.2017.10.021](#).
- [23] R.H. Mohammed, O. Mesalhy, M.L. Elsayed, R. Huo, M. Su, L.C. Chow, Performance of desiccant heat exchangers with aluminum foam coated or packed with silica gel, Appl. Therm. Eng. 166 (2020) 114626. [j.applthermaleng.2019.114626](#).
- [24] K. Nawaz, S.J. Schmidt, A.M. Jacobi, Effect of catalyst and substrate on the moisture diffusivity of silica-aerogel-coated metal foams, Int. J. Heat Mass Transf. 73 (2014) 634–644. [j.ijheatmasstransfer.2014.02.048](#).
- [25] J. Khedari, R. Rawangkul, W. Chimchavee, J. Hirunlabh, a. Watanasungsut, Feasibility study of using agriculture waste as desiccant for air conditioning system, Renew. Energy. 28 (2003) 1617–1628. [S0960-1481\(03\)00003-X](#).
- [26] H. Wang, K.C. Sheng, T. Lan, M. Adl, X.Q. Qian, S.M. Zhu, Role of surface treatment on water absorption of poly(vinyl chloride) composites reinforced by Phyllostachys pubescens particles, Compos. Sci. Technol. 70 (2010) 847–853. [compscitech.2010.01.023](#).
- [27] J. Castillo-gonzález, F. Comino, F.J. Navas-Martos, M. Ruiz de Adana, Life cycle assessment of an experimental solar HVAC system and a conventional HVAC system, Energy Build. 256 (2022) 111697. [j.enbuild.2021.111697](#).
- [28] N. Karnik, U. Bora, K. Bhadri, P. Kadambi, P. Dhatrak, A comprehensive study on current and future trends towards the characteristics and enablers of industry 4.0, J. Ind. Inf. Integr. 27 (2022). [j.jii.2021.100294](#).
- [29] E. Molero, J.J. Fernández, O. Rodríguez-Alabanda, G. Guerrero-Vaca, P.E. Romero, Use of data mining techniques for the prediction of surface roughness of printed parts in polylactic acid (PLA) by fused deposition modeling (FDM): a practical application in frame glasses manufacturing, Polymers (Basel). 12 (2020), <https://doi.org/10.3390/POLYM12040840>.
- [30] B. Redwood, F. Schöffer, B. Garret, *The 3D Printing Handbook*, 3D Hubs B.V., Amsterdam, 2018.
- [31] P.E. Romero, J. Arribas-Barrios, O. Rodriguez-Alabanda, R. González-Merino, G. Guerrero-Vaca, Manufacture of polyurethane foam parts for automotive industry using FDM 3D printed molds, CIRP J. Manuf. Sci. Technol. 32 (2021) 396–404. [j.cirpj.2021.01.019](#).
- [32] A. Pereira, A.F.P. Ferreira, A.E. Rodrigues, A.M. Ribeiro, M.J. Regufe, Additive manufacturing for adsorption-related applications—a review, J. Adv. Manuf. Process. 4 (2022) 1–30, <https://doi.org/10.1002/amp.2.10108>.
- [33] I. Kaur, P. Singh, State-of-the-art in heat exchanger additive manufacturing, Int. J. Heat Mass Transf. 178 (2021) 121600. [j.ijheatmasstransfer.2021.121600](#).
- [34] J. Ning, X. Wang, Y. Sun, C. Zheng, S. Zhang, X. Zhao, C. Liu, W. Yan, Experimental and numerical investigation of additively manufactured novel compact plate-fin heat exchanger, Int. J. Heat Mass Transf. 190 (2022) 122818. [j.ijheatmasstransfer.2022.122818](#).
- [35] A.S. Sabau, A. Bejan, D. Brownell, K. Gluesenkamp, B. Murphy, F. List, K. Carver, C. R. Schaich, J.W. Klett, Design, additive manufacturing, and performance of heat exchangers with a novel flow-path architecture, Appl. Therm. Eng. 180 (2020) 115775. [j.applthermaleng.2020.115775](#).
- [36] B. Ahmadi, S. Bigham, Performance evaluation of hi-k lung-inspired 3d-printed polymer heat exchangers, Appl. Therm. Eng. 204 (2022) 117993. [j.applthermaleng.2021.117993](#).
- [37] U. Puttur, M. Ahmadi, B. Ahmadi, S. Bigham, A novel lung-inspired 3D-printed desiccant-coated heat exchanger for high-performance humidity management in buildings, Energy Convers. Manag. 252 (2022) 115074. [j.enconman.2021.115074](#).

- [38] D. Saltzman, M. Bichnevicius, S. Lynch, T.W. Simpson, E.W. Reutzel, C. Dickman, R. Martukanitz, Design and evaluation of an additively manufactured aircraft heat exchanger, *Appl. Therm. Eng.* 138 (2018) 254–263. j.applthermaleng.2018.04.032.
- [39] M. Alsulami, M. Mortazavi, S.A. Niknam, D. Li, Design complexity and performance analysis in additively manufactured heat exchangers, *Int. J. Adv. Manuf. Technol.* 110 (2020) 865–873, <https://doi.org/10.1007/s00170-020-05898-3>.
- [40] S.C. Daminabo, S. Goel, S.A. Grammatikos, H.Y. Nezhad, V.K. Thakur, Fused deposition modeling-based additive manufacturing (3D printing): techniques for polymer material systems, *Mater Today Chem.* 16 (2020) 100248. j.mtchem.2020.100248.
- [41] ISO Standards, Plastics-Determination of Water Absorption; ISO 62:2008, 61010-1 © Iec:2001. 2008 (2008).
- [42] K.B. Adhikary, S. Pang, M.P. Staiger, Long-term moisture absorption and thickness swelling behaviour of recycled thermoplastics reinforced with *Pinus radiata* sawdust, *Chem. Eng. J.* 142 (2008) 190–198. j.cej.2007.11.024.
- [43] D. Systemes, SolidWorks Software, Solidworks, 2021.
- [44] Ultimaker, Ultimaker Cura, Ultimaker, 2020.
- [45] H.A. Mohammed, P. Gunasegaran, N.H. Shuaib, Influence of channel shape on the thermal and hydraulic performance of microchannel heat sink, *Int. Commun. Heat Mass Transfer.* 38 (2011) 474–480. j.icheatmasstransfer.2010.12.031.
- [46] A.A. Alfaryjat, H.A. Mohammed, N.M. Adam, M.K.A. Ariffin, M.I. Najafabadi, Influence of geometrical parameters of hexagonal, circular, and rhombus microchannel heat sinks on the thermohydraulic characteristics, *Int. Commun. Heat Mass Transfer.* 52 (2014) 121–131. j.icheatmasstransfer.2014.01.015.
- [47] N.S. Nor Arman, R.S. Chen, S. Ahmad, Review of state-of-the-art studies on the water absorption capacity of agricultural fiber-reinforced polymer composites for sustainable construction, *Constr. Build. Mater.* 302 (2021). j.conbuildmat.2021.124174.
- [48] S. Pujari, A. Ramakrishna, K. Tbalarampadal, Comparison of ANN and Regression Analysis for Predicting the Water Absorption Behaviour of Jute and Banana Fiber Reinforced Epoxy composites Selection and peer-review under responsibility of Conference Committee Members of 5th International Conference of Materials Processing and Characterization (ICMPC 2016), 2017. <www.sciedirect.com/www.materialstoday.com/proceedings>.
- [49] J.R. Robledo-Ortíz, M.E. González-López, D. Rodríguez, J.F. Gutiérrez-Ruiz, F. Prezas-Lara, A.A. Pérez-Fonseca, Improving the compatibility and mechanical properties of natural fibers/green polyethylene biocomposites produced by rotational molding, *J. Polym. Environ.* 28 (2020) 1040–1049, <https://doi.org/10.1007/s10924-020-01667-1>.
- [50] R.S. Chen, M.H. Ab Ghani, M.N. Salleh, S. Ahmad, M.A. Tarawneh, Mechanical, water absorption, and morphology of recycled polymer blend rice husk flour biocomposites, *J. Appl. Polym. Sci.* 132 (2015), <https://doi.org/10.1002/app.41494>.
- [51] F. Comino, F. Táboas, F. Peci, M. Ruiz de Adana, Detailed experimental analysis of the energy performance of a desiccant wheel activated at low temperature, *Appl. Therm. Eng.* 178 (2020) 115580. j.applthermaleng.2020.115580.